

**Considerations of Pulsed Raman Spectroscopy for the Analysis of Ocean World Analog Samples.** L. E. Rodriguez<sup>1</sup>, A. G. Yanchilina<sup>2</sup>, Scott M. Perl<sup>1</sup>, K. H. Simon<sup>2</sup>, E. J. Eshelman<sup>2</sup>, C. Sudlik<sup>2</sup>, O. Pochettino<sup>2</sup>, D. S. Kelley<sup>3</sup>, P. S. Sobron<sup>2</sup>, L. M. Barge<sup>1</sup>. <sup>1</sup>Jet Propulsion Laboratory, California Institute of Technology, 4800 Oak Grove Drive, Pasadena, CA, 91109 (Laura.Rodriguez@jpl.nasa.gov), <sup>2</sup>Impossible Sensing, St. Louis, Missouri, <sup>3</sup>School of Oceanography, University of Washington, Box 357940, Seattle, WA 98195, USA.

**Introduction:** Ocean worlds are prime targets in the search for extraterrestrial life as they have an abundance of liquid water [1]. If water-rock interactions are ongoing, precipitation of hydrothermal vents may be ongoing. In Earth's oceans, hydrothermal vents are hotspots of geochemical and biological activity, which may have generated conditions that facilitated abiogenesis on a prebiotic world [2, 3]. Hence, hydrothermal vents on ocean worlds are a promising locale to search for extraterrestrial life.

In this work we explored the feasibility of using a pulsed Raman system to characterize the mineralogy and organic geochemistry of hydrothermal vent samples to deduce its feasibility for underwater exploration of ocean worlds. Pulsed Raman is of particular interest as it can be easily coupled with Laser Induced Breakdown Spectroscopy (LIBS) and time-resolved fluorescence (i.e., SuperCam on Perseverance), however because it requires timing of the electronics it does add technical risk to the instrument payload.

**Methods:** Samples from the Roane chimney in the Mothra Hydrothermal Field (Juan de Fuca Ridge), standards for minerals commonly found at such sites, and other astrobiologically relevant organic/inorganic standards were analyzed using a Raman (Dual in-situ Spectroscopy and coring (DiSCO)) system specifically designed for space flight by Impossible Sensing. DiSCO employs a 1064 nm pulsed fiber optic laser that is frequency-doubled to give a 515 nm laser. Both rough and high resolution (6 x 6 mm and 1 x 1mm) maps were generated using a liquid lens that enables auto-focusing of the laser without the use of any movable parts [4]. Preprocessing (background subtraction, baseline correction, denoising) and data analysis of the spectra were carried out using R software. To confirm elemental, mineralogical, and organic trends, pieces of select hydrothermal vent samples were sent to Activation Laboratories, Ltd. (Actlabs) in Toronto, Ontario to determine total carbon (TC), total inorganic carbon (TIC), and total organic carbon (TOC) content and perform Inductively coupled plasma atomic emission spectroscopy and X-ray diffraction (XRD) analysis.

**Results:** *Iron oxyhydroxides and sulfides.* The Raman signal of any pellets containing iron was significantly reduced and noisy. Pulsed Raman rapidly transformed both iron oxyhydroxides and sulfides upon analysis, generating similar-looking spectra with a

broad peak at 846 cm<sup>-1</sup> and a sharp peak at 2338 cm<sup>-1</sup>; these peaks are not expected for iron oxyhydroxides or sulfides and do not match the RRUFF spectra of the corresponding mineral. Thus, these minerals would be difficult to identify and distinguish using the current system; the only notable difference between them being the shape of the 846 cm<sup>-1</sup> peak, likely due to the presence or absence of an unresolved peak (Fig. 1). Notably, the 846 cm<sup>-1</sup> peak is the same as that expected of ferrate (Fe(IV)O<sub>4</sub>), metal-OH bending vibrations, or Si-O-Si vibrations as seen in silicates. The 2338 cm<sup>-1</sup> is attributed to atmospheric N<sub>2</sub>.

*Phosphorus compounds.* Pellets of inorganic P species (phosphate, phosphite, pyrophosphate, triphosphate, and trimetaphosphate) generated moderately-strong Raman signals and unique spectra with multiple peaks. However, the pellet resulting from phosphate co-precipitated with Fe(II) (likely vivianite given its green color) did not generate any distinguishing PO<sub>4</sub> peaks or any peaks other than those at 846 and 2338 cm<sup>-1</sup> which are present in any samples containing significant amounts of iron. Finally, Raman shifts due to the phosphate groups of organophosphates (AMP, ADP, ATP, and glycerol-phosphate) were occasionally detectable, but significantly dampened compared to shifts from the attached organic and/or fluorescence.

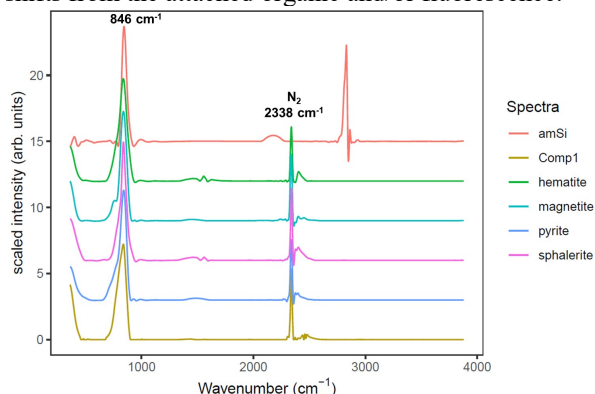


**Figure 1.** Spectra of mineral standards analyzed with DiSCO. Note that the spectra from the iron minerals are almost indistinguishable and do not match their corresponding spectra in the RRUFF database. This suggests that the minerals are being transformed by the laser during analysis. amSi = amorphous silica; Comp1 = MCR component 1 identified as iron mineral(s), the majority of which is likely pyrite (see *Raman Mapping* in Results).

*Organics.* Pellets of the following organics were analyzed: ferricyanide, urea, pyrene, adenine, glucose,

lactose, and glyoxylate. Shifts characteristic of C-H, C-C, esters, O-H, N-C-N, and N-H groups were easily observed, with the sharpest peaks coming from pyrene and urea. Like other samples containing Fe, the spectra of ferricyanide was very weak and noisy and included the two peaks at 846 and 2338  $\text{cm}^{-1}$ ; however, unlike the other iron samples, there was an additional peak at 2140  $\text{cm}^{-1}$  from the C-N stretching mode. To determine whether these organics would be discernable in natural samples, we doped a mixture of organics representing the chemical and molecular composition of a typical cell with pulverized vent precipitates from the most interior and exterior portions of the Roane chimney. The resulting mixtures were pelleted and analyzed using DiSCO. Preliminary analysis suggests that peaks diagnostic of organics are severely dampened due to fluorescence; dampening by the surrounding iron matrix is also likely another factor as observed with our standards. Indeed, attempts to decipher Raman peaks diagnostic of organic matter using Partial Least Squares Regression (PLS-R) were only mildly successful: with the exception of 1 peak whose shift matched that of a carbonyl group (1691  $\text{cm}^{-1}$ ), the shifts identified as most predictive of organic carbon were those inversely correlated with organic content – that is, those corresponding to the mineral matrix which decreased in wt% as organic content increased rather than shifts corresponding to the organics themselves. Alternatively, we are investigating whether the fluorescence profile (shape, intensity, width, etc.), originally removed during our preprocessing steps, could provide more reliable features directly correlated with organic content.

**Raman mapping.** We analyzed the surfaces of samples cut from the Mothra vent so that we could evaluate whether pulsed Raman can sufficiently capture the geochemical, and potentially organic, gradients within the precipitate. The abundance and pure Raman spectra of major components contributing to the differences between the interior and exterior portions of the chimney were discerned using Multivariate Curve Resolution (MCR) [5]. Nine major components were deconvolved; comparisons with Raman spectra collected from standards allowed us to identify barite, an iron mineral(s) (determined to be predominately pyrite, but likely also includes some contributions from sphalerite and chalcocopyrite based off its known abundance from XRD and previous analysis using LIBS and SEM [6-8]); anhydrite was also identified in trace amounts in the most exterior portion of the chimney. These MCR components were then used to generate heat maps of the various minerals with depth into the chimney (Fig. 2). The relative abundances of these minerals are in agreement with previous work. Notably, mapping MCR compo-

nents is more informative than mapping a single or pair of peaks whose intensity may be due to several mineral or organic species.

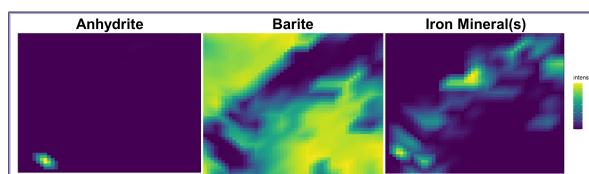


**Figure 2.** Maps produced from the most exterior portion of the chimney using three of the major components predicted from MCR and identified as anhydrite, barite, and an iron mineral (predicted to be predominately pyrite). Note that this sample surface is mostly barite; it appears that sometime after the barite precipitated hydrothermal fluid passed through, resulting in the iron mineral vein seen in the left most image. Scale bar is relative intensity.

**Conclusions:** Pulsed Raman spectroscopy (515 nm) can easily distinguish between phosphorus species and preserves the organic shifts diagnostic of various functional groups in organic compounds. However, the technique transforms/degrades iron oxyhydroxides, iron phosphate, and iron/metal sulfides such that they are nearly indistinguishable and cannot be confirmed by comparison with the RRUFF database. Moreover, the presence of iron severely dampens the Raman signal, even for iron-organometallic compounds such as ferricyanide. Given that iron is one of the most abundant elements expected in the rocky crust of ocean worlds, and is prevalent in different forms within hydrothermal vent precipitates, exploration of oceanic environments with pulsed Raman may be severely hindered in the absence of orthogonal techniques such as LIBS and time-resolved fluorescence. Nonetheless, coupling multivariate analysis with Raman we were able to identify major mineralogical components (anhydrite, barite, and an iron component [which we know to be predominantly pyrite] in our vent precipitates. The identification of the other major components is ongoing.

**Acknowledgments:** This work was performed at the Jet Propulsion Laboratory, California Institute of Technology under a contract with NASA (80NM0018D004) and was supported by the NASA PSTAR grant #80NSSC18K1651.

**References:** [1] Hendrix A. R. et al. (2019) *Astrobiology*, 19, 1–27. [2] Russell M. J. et al. (2014) *Astrobiology*, 14, 308–343. [3] Martin W. et al. (2008) *Nat. Rev. Microbiol.*, 6, 805–814. [4] Yanchilina A. et al. (2021) *52<sup>nd</sup> LPSC*, Abstract #2662. [5] Haddad J. E. et al. (2019) *Miner. Eng.* 134, 281–290. [6] Kristall B. et al. (2006) *Geochem. Geophys. Geosyst.*, 7, Q07001. [7] Kristall B. et al. (2011) *Chem. Geol.* 290, 12–30. [8] Rodriguez et al. 2022, *in prep.*